UDC 621.354

THE COMPENSATION TOPOLOGIES STUDY OF THE DYNAMIC WIRELESS CHARGING SYSTEM FOR THE UNDERGROUND SUSPENDED MONORAIL

Valery M. Zavyalov[1,2], Irina Yu. Semykina[2], Sergey A. Abeidulin[1], Nikolay M. Shaitor[1], Gennady M. Lebedev[2]

[1] Sevastopol State University
[2] T.F. Gorbachev Kuzbass State Technical University

CC BY

Article info
Received:
11 March 2026

Revised:
02 June 2026

Accepted:
03 July 2026

Keywords: electric vehicle, underground suspended monorail, dynamic wireless charging system, wireless power transfer, compensation topology, battery, equivalent load, transmitting line, efficiency, transfer function, analytic hierarchy process

Abstract.
The development of electric transport and its charging infrastructure is cutting-edge, including for industrial applications. Underground suspended monorail is a mining transport that is also trending to implement battery-powered locomotives. The promising way for their charging is using a dynamic wireless charging system built with a long line on the transmitting side. For such systems, the influence of compensation topology on the operation quality is poorly studied. The article investigates four two-element topologies. As the performance indicators, the following are chosen: the efficiency of wireless power transfer and the transmission ratio, which shows the ratio of the resonant circuit output voltage, indicating the load voltage, to the resonant circuit input voltage. For each topology, the mathematical model is compiled and the parametric equations describing the performance indicators are obtained. An analysis of the performance indicators of the dynamic wireless charging system with different compensation topologies was made, taking into account the features of the underground suspended monorail. Based on the obtained results using the analytic hierarchy process, the best topology for the conditions under consideration was selected.

For citation Zavyalov V.M., Semykina I.Yu., Abeidulin S.A., Shaitor N.M., Lebedev G.M. The compensation topologies study of the dynamic wireless charging system for the underground suspended monorail. *Journal of mining and geotechnical engineering.* 2026;3(34):4-25. DOI: 10.26730/2618-7434-2026-2-4-25, EDN: HKQZIL

Acknowledgments: the research was supported by the state assignment of Ministry of Science and Higher Education of the Russian Federation (№ 075-03-2024-082-2).

Introduction

One of the modern development areas of science and technology is energy saving and anthropogenic load reduction [1] which includes research in the field of electric transport. The vehicle-to-grid (V2G) concept takes a prominent position where. For electric transport it allows, among others, to adjust the power consumption profile and reduce peak demand for electricity [2, 3]. The V2G concept contains many components, such as electric vehicle motion control systems [4], battery monitoring systems [5], charging infrastructure [6], etc. Charging infrastructure is a key link between electric vehicles and power supply networks and can be wired and wireless [7–9]. Compared to wired ones, wireless charging systems [10], in addition to influencing energy efficiency, also contribute to increasing

DOI: 10.26730/2618-7434-2026-3-4-25

the autonomy of electric transport. This advantage makes it urgent for hazardous industries and promises to proceed from manned to unmanned technologies.

An industry where unmanned technologies are extremely relevant is underground mining. A lot of research is being conducted in this area. For example, the study [11] describes the implementation of unmanned technologies at an underground mine in China. It should be noted that diesel loaders were used there, although in underground mining there is a trend to substitute diesel transport with battery-powered analogs [12].

Diesel transport is also widely used in Russian mines. For example, a suspended monorail with diesel locomotives that used on a horizontal plane and inclinations up to ±30° [13]. There are also battery-powered locomotives, for example [14, 15]. Such equipment although promising but less common. For this reason, it would be rational to consider more advanced options for its charging, namely a dynamic wireless charging system (DWCS) that allows on-moving recharge locomotive's battery.

Systems with a similar operating principle have been known for mining since 1995 [16], but they are supposed to transfer power directly to drive motors rather than batteries. The system [17] can be considered a prototype of DWCS for the underground suspended monorail. It has a long line on the transmitting side rather than an array of transmitting coils like in [18–21]. The system under consideration consists of a transmitter and a receiver and includes a high-frequency inverter that supplies a resonant circuit with a transmitting line L_1, a receiving coil L_2, and a rectifier that transfers energy from a resonant circuit to a charge controller that supplies the battery *GB* and controls its operating parameters during charging and discharging. The transmitting line can be located on the monorail, and the receiving coil is placed on the surface of the battery container (Fig. 1).

The resonant circuit includes compensation elements, without which the transfer of even a small current would be with a large amount of reactive power that makes an additional load on the high-frequency inverter and limits the amount of active power transferred [22]. Many studies are devoted to possible compensation topologies and their properties [23–28], but the vast majority consider static wireless charging systems.

DWCS of the considered type substantially differs from static ones. The receiving coil, taken in this study as flat and rectangular, moves along the transmitting line with the locomotive. Due to the design, the inductive coupling between the transmitting line and the receiving coil is weak.

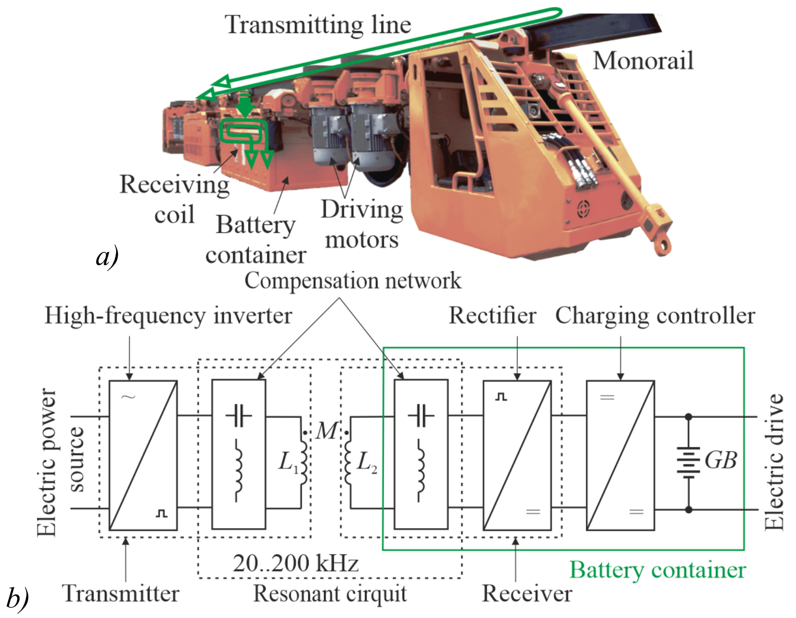

Fig. 1. DWCS for the underground suspended monorail: a) concept; b) block diagram
Рис. 1. Динамическая система беспроводного заряда (ДСБЗ) для подземной подвесной монорельсовой дороги: а) концепция; б) блок-схема

The main electric load of battery-powered locomotives is the drive motors, and power consumption from the DWCS varies significantly and depends on the battery charge level, the loading of the monorail transport, acceleration when starting and stopping, etc. Hence, the voltage at the rectifier output should be constant. Taking these factors into account, the system under consideration will have the following features:

1. Since the length of the transmitting line depends on the technological scheme of monorail transport and can change as mining operations progress, the inductance of the transmitting line L_1 can correspondently change;

2. When maintaining the constant rectifier output voltage, load changes of the battery-powered locomotive can be described as changes in the equivalent load of the battery and the electric drive R_{load};

3. The mutual inductance M between the transmitting line and the receiving coil is mainly defined by the interaction between the receiving coil and the section of the transmitting line located in the vicinity of the receiving coil and has a relatively small value compared to the self-inductances of the transmitting line L_1 and the receiving coil L_2. During the locomotive movement, a slight change in the coils' relative position is possible, contributing to a slight change in M. However, if the transmitting line is poorly fastened to the monorail, sagging is possible. When the receiving coil is near such sagging the mutual inductance M increases significantly.

Therefore, for DWCS, it is necessary to analyze the performance indicators depending upon the compensation topology under changes in R_{load}, L_1, and M analogically to [25, 26].

Theory

As a research tool, frequency domain analysis employing transfer functions is used. This method is chosen because a transfer function being an input-output relation can be considered as a transient parameter. For example, if a voltage is an input and a current is an output, such a transfer function represents a transient conductance.

This tool requires that the object is linear, and therefore the following basic assumptions were made for DWCS:

- the equivalent load of the battery and the electric drive R_{load} is active load;
- the high-frequency inverter and the high-voltage bridge rectifier are ideal, which means there are no nonlinear distortions of currents and voltages, as well as no switching and conductive losses in the semiconductor switches;
- the dielectric losses in resonant circuit capacitors is not considered;
- At high frequencies, the skin effect has a negligible impact on the coil's inductance and does not result in additional ohmic losses associated with current displacement.

The following were chosen as the main performance indicators of DWCS:

1) the efficiency η of wireless power transfer;

2) the transmission ratio A_U, showing the ratio of the resonant circuit output voltage, indicating the load voltage, to the resonant circuit input voltage.

The efficiency η might be expressed as:

$$\eta = \frac{P_{load}}{P_{in}}, \tag{1}$$

where P_{load} is the power delivered to the load; P_{in} is the power consumed from the input.

The transmission ratio A_U might be expressed as:

$$A_U = \frac{|u_2|}{|u_1|}, \tag{2}$$

where u_1 is the resonant circuit input voltage; u_2 is the resonant circuit output voltage.

There is a great variety of compensation topologies. This analysis considered four variants of the two-element compensation topologies with one capacitor installed in the transmitting (receiving) side additionally with the transmitting (receiving) coil:

- Series-Series (SS) topology;
- Series-Parallel (SP) topology;

– Parallel-Series (PS) topology;
– Parallel- Parallel (PP) topology.

DWCS with any topology can be supplied from either a voltage or a current source. In practice, when compensation topology has the series-connected capacitor on the transmitting side, the voltage source is more often used, and the current source is used in the case of the parallel-connected capacitor.

Idealized equivalent circuits of DWCS with the considered topologies is shown at Fig. 2, where u_{in} is the source voltage that for SS and SP topologies is equal to u_1; u_{C1} is the capacitor voltage at the primary side that for PS and PP topologies is equal to u_1; u_{C2} is the capacitor voltage at the secondary side that for SP and PP topologies is equal to u_2; i_{in} is the source current; i_{load} is the load current; i_1 is the transmitting circuit current; i_2 is the receiving circuit current that for SS and PS topologies is equal to i_{load}; i_{C1} is the capacitor current at the primary side; i_{C2} is the capacitor current at the secondary side; R_1, R_2, C_1, C_2 are primary side and secondary side resistance and capacitance consequently.

To analyze the performance indicators of DWCS under changes in the equivalent load resistance R_{load}, the inductance of the transmitting loop L_1, and the mutual inductance M using transfer functions, the following operations for each topology were carried out:

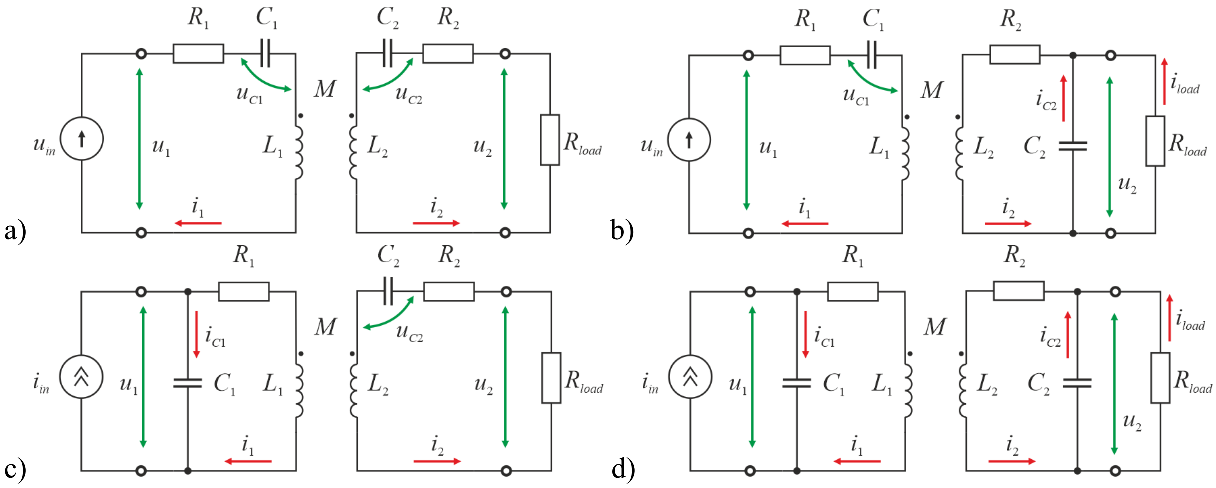

Fig. 2. Idealized equivalent circuits of DWCS with different topologies: a) SS; b) SP; c) PS; d) PP
Рис. 2. Идеализированные эквивалентные схемы ДСБЗ с различными топологиями: a) последовательно-последовательная (SS); b) последовательно-параллельная (SP); c) параллельно-последовательная (PS); d) параллельно-параллельная (PP)

– based on the equivalent circuit, a mathematical model of DWCS has been compiled initially in the form of differential equations and after that using the Laplace transform in operator form;

– The transfer functions have been obtained allowing us to calculate η and A_U after moving to the frequency domain.

As a result, the parametric equations were obtained (Table 1) that relate η and A_U with the parameters R_{load}, L_1, and M of the wireless charging system. The full description of their deriving is placed in the Appendix.

In Table 1 the following notations are used: the values in the operator form are denoted in capital, s is the operator variable, W_x denotes the transfer functions that relate the output value x to the source current or voltage. The transfer functions W_x in the frequency domain are decomposed as follows:

$$W_x(j\omega) = Re(W_x(\omega)) + j\,Im(W_x(\omega)) = A_x(\omega)e^{j\varphi_x(\omega)}, \quad (3)$$

where ω is the angular frequency.

Results and discussion

Parametric analysis

The equations in Table I were used to parametrically analyze DWCS in the frequency domain, both at nominal parameters and under changes in L_1, M, and R_{load}.

DOI: 10.26730/2618-7434-2026-3-4-25

Table 1. Equations for η and A_U calculating
Таблица 1. Уравнения для расчета η и A_U

Value	Topology			
	SS	SP	PP	PS
Efficiency	$\eta=\frac{A^2_{i_{2ss}}(\omega)R_{load}}{\mathrm{Re}\left(W_{i_{1ss}}(\omega)\right)}$	$\eta=\frac{A^2_{i_{load\ sp}}(\omega)R_{load}}{\mathrm{Re}\left(W_{i_{1sp}}(\omega)\right)}$	$\eta=\frac{A^2_{i_{load\ pp}}(\omega)R_{load}}{\mathrm{Re}\left(W_{u_{C1pp}}(\omega)\right)}$	$\eta=\frac{A^2_{i_{2ps}}(\omega)R_{load}}{\mathrm{Re}\left(W_{u_{C1ps}}(\omega)\right)}$
Transmission ratio	$A_U=A_{i_{2ss}}(\omega)R_{load}$	$A_U=A_{i_{load\ sp}}(\omega)R_{load}$	$A_U=\frac{A_{i_{load\ pp}}(\omega)R_{load}}{A_{u_{C1pp}}(\omega)}$	$A_U=\frac{A_{i_{2ps}}(\omega)R_{load}}{A_{u_{C1ps}}(\omega)}$
Transfer functions	$W_{i_{2ss}}(s)=\frac{I_2(s)}{U_1(s)}=$ $=\frac{s^3a_{1ss}}{s^4b_{1ss}+s^3b_{2ss}+s^2b_{3ss}+sb_{4ss}+1}$ $W_{i_{1ss}}(s)=\frac{I_1(s)}{U_1(s)}=$ $=\frac{(s^3a_{2ss}+s^2a_{3ss}+s)a_{4ss}}{s^4b_{1ss}+s^3b_{2ss}+s^2b_{3ss}+sb_{4ss}+1}$	$W_{i_{load\ sp}}(s)=\frac{I_{load}(s)}{U_1(s)}=$ $=\frac{s^2a_{1sp}}{s^4b_{1sp}+s^3b_{2sp}+s^2b_{3sp}+sb_{4sp}+b_{5sp}}$ $W_{i_{1sp}}(s)=\frac{I_1(s)}{U_1(s)}=$ $=\frac{s^3a_{2sp}+s^2a_{3sp}+sa_{4sp}}{s^4b_{1sp}+s^3b_{2sp}+s^2b_{3sp}+sb_{4sp}+b_{5sp}}$	$W_{i_{load\ pp}}(s)=\frac{I_{load}(s)}{I_{in}(s)}=$ $=\frac{sa_{1pp}}{s^4b_{1pp}+s^3b_{2pp}+s^2b_{3pp}+sb_{4pp}+b_{5pp}}$ $W_{u_{C1pp}}(s)=\frac{U_{C1}(s)}{I_{in}(s)}=$ $=\frac{s^3a_{2pp}+s^2a_{3pp}+sa_{4pp}+a_{5pp}}{s^4b_{1pp}+s^3b_{2pp}+s^2b_{3pp}+sb_{4pp}+b_{5pp}}$	$W_{i_{2ps}}(s)=\frac{I_2(s)}{I_{in}(s)}=$ $=\frac{s^2a_{1ps}}{s^4b_{1ps}+s^3b_{2ps}+s^2b_{3ps}+sb_{4ps}+1}$ $W_{u_{C1ps}}(s)=\frac{U_{C1}(s)}{I_{in}(s)}=$ $=\frac{s^3a_{2ps}+s^2a_{3ps}+sa_{4ps}+a_{5ps}}{s^4b_{1ps}+s^3b_{2ps}+s^2b_{3ps}+sb_{4ps}+1}$
Coefficients	$a_{1ss}=-MC_1C_2$ $a_{2ss}=L_2C_2$ $a_{3ss}=(R_2+R_{load})C_2$ $a_{4ss}=C_1$ $b_{1ss}=(L_1L_2-M^2)C_1C_2$ $b_{2ss}=(R_1L_2+(R_2+R_{load})L_1)C_1C_2$ $b_{3ss}=R_1(R_2+R_{load})C_1C_2+$ $+L_1C_1+L_2C_2$ $b_{4ss}=R_1C_1+(R_2+R_{load})C_2$	$a_{1sp}=MC_1$ $a_{2sp}=R_{load}L_2C_1C_2$ $a_{3sp}=\left(R_2R_{load}C_2+L_2\right)C_1$ $a_{4sp}=\left(R_2+R_{load}\right)C_1$ $b_{1sp}=R_{load}\left(L_1L_2-M^2\right)C_1C_2$ $b_{2sp}=R_{load}\left(R_2L_1+R_1L_2\right)C_1C_2+$ $+\left(L_1L_2-M^2\right)C_1$ $b_{3sp}=\left(R_2+R_{load}\right)L_1C_1+R_{load}L_2C_2+$ $+R_1L_2C_1+R_1R_2R_{load}C_1C_2$ $b_{4sp}=R_1\left(R_2+R_{load}\right)C_1+R_2R_{load}C_2+L_2$ $b_{5sp}=R_2+R_{load}$	$a_{1pp}=-M$ $a_{2pp}=R_{load}\left(L_1L_2-M^2\right)C_2$ $a_{3pp}=\left(L_2L_1-M^2\right)+R_{load}\left(R_1L_2+R_2L_1\right)C_2$ $a_{4pp}=R_1L_2+R_2L_1+R_{load}\left(R_1R_2C_2+L_1\right)$ $a_{5pp}=R_1\left(R_2+R_{load}\right)$ $b_{1pp}=R_{load}\left(L_1L_2-M^2\right)C_1C_2$ $b_{2pp}=R_{load}\left(R_1L_2+R_2L_1\right)C_1C_2+\left(L_1L_2-M^2\right)C_1$ $b_{3pp}=R_1R_2R_{load}C_1C_2+R_{load}\left(L_2C_2+L_1C_1\right)+$ $+\left(R_1L_2+R_2L_1\right)C_1$ $b_{4pp}=R_1\left(R_2+R_{load}\right)C_1+R_2R_{load}C_2+L_2$ $b_{5pp}=R_2+R_{load}$	$a_{1ps}=-MC_2$ $a_{2ps}=(L_1L_2-M^2)C_2$ $a_{3ps}=(R_1L_2+\left(R_2+R_{load}\right)L_1)C_2$ $a_{4ps}=R_1\left(R_2+R_{load}\right)C_1+L_1$ $a_{5ps}=R_1$ $b_{1ps}=\left(L_1L_2\text{-}M^2\right)C_1C_2$ $b_{2ps}=\left(R_1L_2+\left(R_2+R_{load}\right)L_1\right)C_1C_2$ $b_{3ps}=L_1C_1+L_2C_2+R_1\left(R_2+R_{load}\right)C_1C_2$ $b_{4ps}=R_1C_1+\left(R_2ER_{load}\right)C_2$

 DOI: 10.26730/2618-7434-2026-3-4-25

As an example, the underground suspended monorail in Fig. 1 was considered. Based on the assessment dimensions of the battery container, on which the rectangular receiving coil is placed, and the length of the transmitting line of 200 m, the inductances L_1, L_2, and M were determined.

The receiving coil and the transmitting line are meant to be made of the high-voltage high-frequency winding wire LELOR-E with a nominal cross-section of 50 mm^2 and a maximum diameter of 15 mm. Based on the specific resistance of LELOR-E the resistances R_1, R_2 were determined. The equivalent load resistance was chosen based on the parameters of a lithium-ion battery with a nominal voltage of 130 V and a nominal charging current of 260 A. The capacitances of the compensation capacitors were selected from the ratio:

$$\frac{1}{\sqrt{L_1C_1}} = \frac{1}{\sqrt{L_2C_2}} = \omega_r, \tag{4}$$

where ω_r is the resonant frequency at which the system should operate taken to be $2\pi\cdot 50\cdot 10^3$ rad/s (50 kHz). Thus, the nominal parameters of the considered DWCS are given in Table 2.

Table 2. The nominal parameters of DWCS for the underground suspended monorail
Таблица 2. Номинальные параметры ДСБЗ для подземной подвесной монорельсовой дороги

L_1, μH	L_2, μH	M, μH	R_1, Ω	R_2, Ω	R_{load}, Ω	ω_r, 10^5·rad/s	C_1, nF	C_2, nF
440	58	1.75	0.5	0.004	0.5	3.14	23.05	174.8

The efficiency η and the transmission ratio A_U in the frequency domain under normal conditions are shown in Fig. 3. All curves on the plot have a clearly expressed resonance at the frequency ω_r. It should be noted that the curves $\eta(\omega)$ have overlap for the pair of SS and PS topologies and the pair of SP and PP topologies. The curves $A_U(\omega)$ are of the same order of magnitude for the pair of SS and SP topologies and the pair of PS and PP topologies. Because η and A_U in are negligibly small out of ω_r, further parametric analysis was carried out only at the resonant frequency.

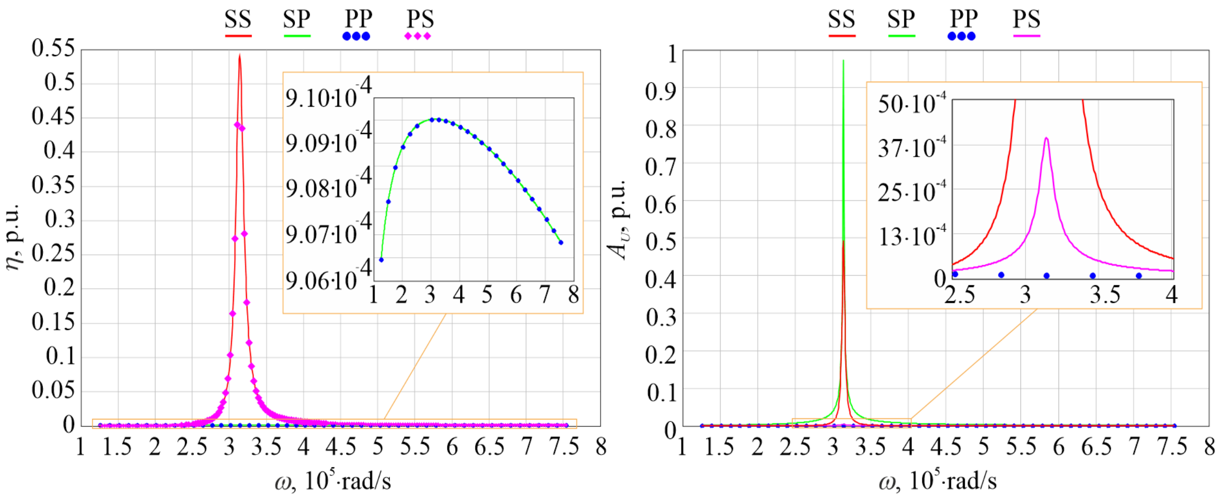

Fig. 3. The performance indicators of DWCS at the normal conditions
Рис. 3. Показатели эффективности ДСБЗ в нормальных условиях

Analyzing the impact of changes in the equivalent resistance of the battery and the electric drive, only R_{load} has been varied in the equations from Table 1 for each topology. The range of R_{load} variations was chosen to assess η and A_U in both the normal conditions and the boundaries, which are no-load with R_{load} increased by 200 times and short-circuit with R_{load} reduced by 200 times. The obtained $\eta(R_{load})$ and $A_U(R_{load})$ are shown in Fig. 4.

DOI: 10.26730/2618-7434-2026-3-4-25

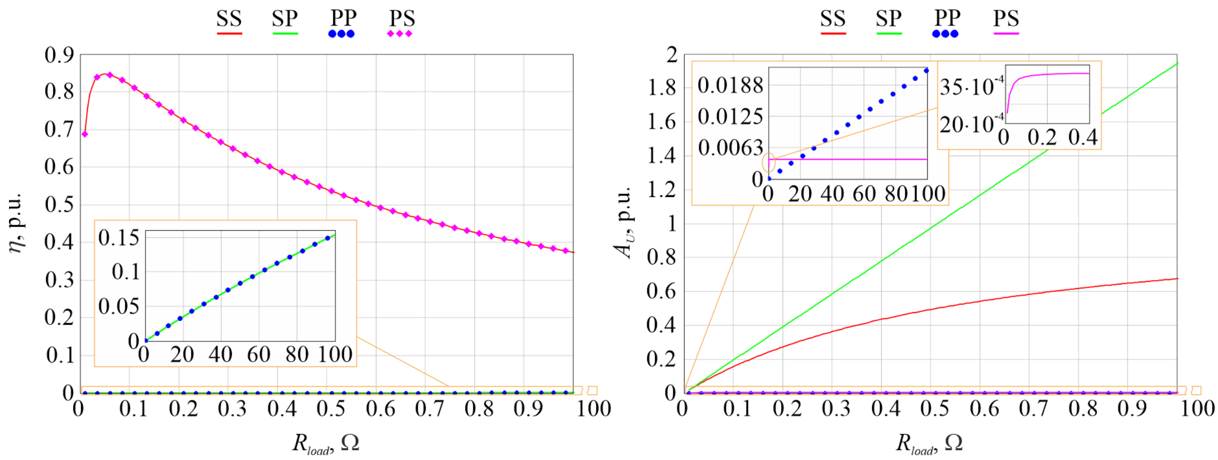

Fig. 4. The performance indicators at the resonant frequency under R_{load} changes
Рис. 4. Показатели эффективности на резонансной частоте при изменении R_{load}

For the pair of SS and PS topologies and the pair of SP and PP topologies, the curves $\eta(R_{load})$ have a different character. In the first case, η smoothly decreases with the growth of R_{load} but drops sharply in the vicinity of short-circuit. In the second case, an increase in R_{load} leads to a virtually linear increase in η. A similar is true for $A_U(R_{load})$. An increase in R_{load} comes with a linear increase in A_U for SP and PP topologies but with an exponential saturation of A_U for SS and PS topologies. It is notable that in the vicinity of normal conditions, the value of A_U for PS becomes virtually constant.

Analyzing the impact of changes in the mutual inductance between the transmitting line and the receiving coil, it was assumed that a slight change in the coils' relative position might cause a slight decrease in M, but in the case of sagging M increases significantly. Hence, the range of M variations in the equations from Table I was selected from –0.5 to +15 times relative to the nominal value. The obtained $\eta(M)$ and $A_U(M)$ are shown in Fig. 5.

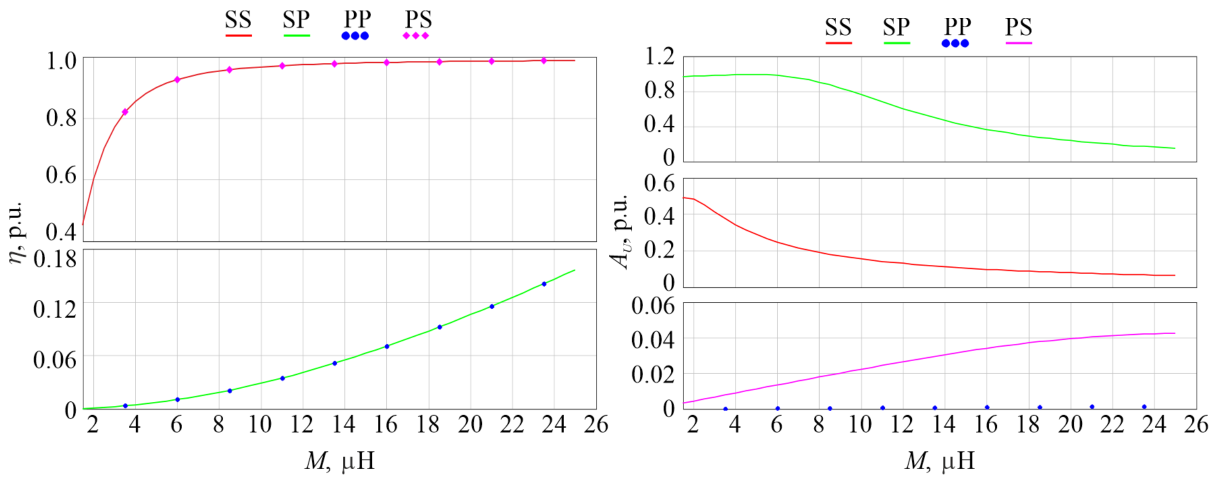

Fig. 5. The performance indicators at the resonant frequency under M changes
Рис. 5. Показатели эффективности на резонансной частоте при изменении M

An increase in M leads to an increase in η for all topologies, but for the SS and PS topologies, this increase is of exponential saturation nature. As for A_U, the curves $A_U(M)$ have a different character for the pair of SS and SP topologies and the pair of PS and PP topologies. In the first case, an increase in M leads to an increase in A_U, but in the second case, the trend is the opposite because of bifurcation. The bifurcation phenomenon is when the input impedance of the wireless charging system changes its nature from capacitive to inductive, and hence, in the frequency domain, the extremum at ω_r splits into two extrema to the left and right of ω_r [29, 30]. It should be noted that for SS and SP topologies the value of A_U even reduced due to bifurcation is significantly higher than for PS and PP topologies.

Analyzing the impact of the transmission line prolongation as mining operations progress, in the equations from Table I not only L_1 has been varied for each topology but also R_1 due to prolongation of the wire and C_1 due to maintaining the resonant frequency ω_r constant according to (4). The range of L_1 variations was chosen so that the prolongation multiplicity of the transmission line is from –1/2 to +2. The obtained $\eta(L_1)$ and $A_U(L_1)$ are shown in Fig. 6.

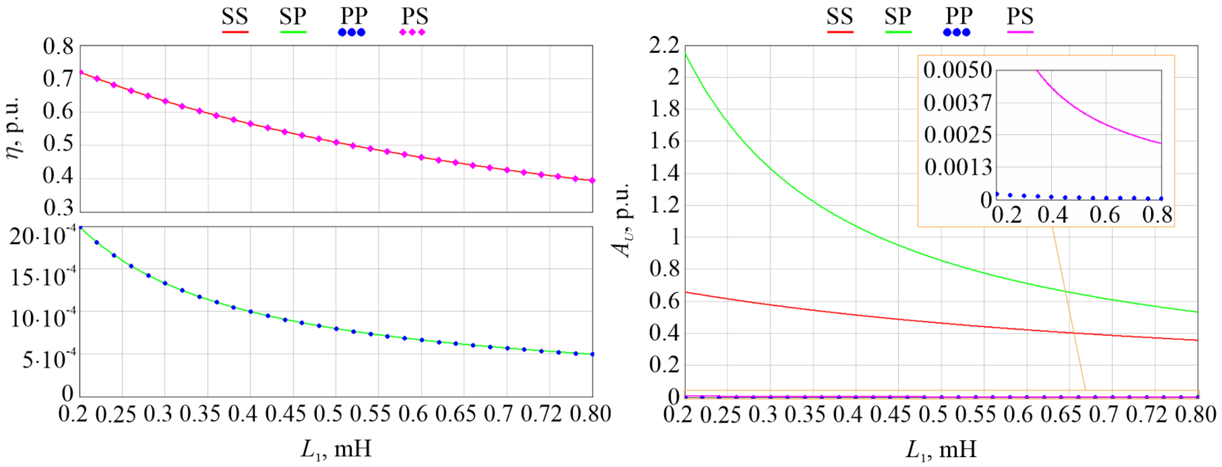

Fig. 6. The performance indicators at the resonant frequency under L_1 changes by the transmission line prolongation
Рис. 6. Показатели эффективности на резонансной частоте при изменении L_1 в результате удлинения передающей линии

For all topologies, both η and A_U show an inverse dependence on L_1, which indicates the limit existed for the rational length of the transmitting line. This means that DWCS with a high working length requires sectioning of the transmitting equipment.

Comparative analysis

The analytic hierarchy process can be used to compare the compensation topologies of DWCS for the underground suspended monorail [31, 32]. The method assumes pairwise comparisons of the compensation topologies relating to all decision criteria, which are given in Table 3.

Table 3. Hierarchy of decision criteria
Таблица 3. Иерархия критериев

First level		Second level		Technical meaning
Desig-nation	Performance indicator	Desig-nation	Conditions	
K1	η	K1.1	Normal	Determines the efficiency of wireless power transfer, and therefore the energy consumed by DWCS from the grid
		K1.2	R_{load} changes	Is sufficient η ensured when changing loads, typical for the underground suspended monorail (starting, stopping, etc.)?
		K1.3	M changes	Is sufficient η ensured when sagging on the transmitting line caused by poorly fastening to the monorail?
		K1.4	L_1 changes	Is sufficient η ensured when the transmission line prorogates as mining operations progress?
K2	A_U	K2.1	Normal	Determines the voltage class of the semiconductor switches of the high-frequency

First level		Second level		Technical meaning
Desig-nation	Performance indicator	Desig-nation	Conditions	
				inverter and rectifier and how technically difficult maintaining a constant voltage at the rectifier output
		K2.2	R_{load} changes	Does DWCS ensure a constant u_2 when changing loads, typical for the underground suspended monorail (starting, stopping, etc.)?
		K2.3	M changes	Does DWCS ensure a constant u_2 when sagging on the transmitting line caused by poorly fastening to the monorail?
		K2.4	L_1 changes	Does DWCS ensure a constant u_2 when the transmission line prorogates as mining operations progress?

Since the parametric analysis was performed on a specific example and the parameters of DWCS in real conditions may differ, the use of quantitative assessment is not correct and hence the seventeen-digit Saaty scale [31] was used to compile the paired comparison matrixes (PCM). To illustrate the method, let us consider the decision criteria K1.1 and K2.2.

Start from K1.1. Since for DWCS under consideration the topologies SP and PP have such a low efficiency at the resonant frequency that their implementation is impractical to a very great degree, the topologies SS and PS have absolute superiority, and the pair of SP and PP topologies and the pair of SS and PS are equivalent. Thus, PCM relating to K1.1 becomes:

$$C_{\text{K1.1}} = \begin{pmatrix} 1 & 9 & 9 & 1 \\ 1/9 & 1 & 1 & 1/9 \\ 1/9 & 1 & 1 & 1/9 \\ 1 & 9 & 9 & 1 \end{pmatrix} \begin{vmatrix} \text{SS} \\ \text{SP} \\ \text{PP} \\ \text{PS} \end{matrix}. \quad (5)$$

The next is K2.2. The power sources of DWCS have limited parameters because regardless of technical solution the upper-level power source is always the power grid with specific power and voltage limits. Hence, the value of A_U should tend to be unity or higher to maintain u_2. Considering the curves $A_U(R_{load})$ shown in Figure 4, SP topology has a slight advantage over SS topology, just as PP over PS, while SP has absolute superiority over PS. Thus, PCM relating to K2.2 becomes:

$$C_{\text{K2.2}} = \begin{pmatrix} 1 & 1/2 & 7 & 8 \\ 2 & 1 & 8 & 9 \\ 1/7 & 1/8 & 1 & 2 \\ 1/8 & 1/9 & 1/2 & 1 \end{pmatrix} \begin{vmatrix} \text{SS} \\ \text{SP} \\ \text{PP} \\ \text{PS} \end{vmatrix}. \quad (6)$$

Similarly, PCMs were obtained for all second-level decision criteria from Table III:

$$C_{\text{K1.2}} = \begin{pmatrix} 1 & 8 & 8 & 1 \\ 1/8 & 1 & 1 & 1/8 \\ 1/8 & 1 & 1 & 1/8 \\ 1 & 8 & 8 & 1 \end{pmatrix} \begin{vmatrix} \text{SS} \\ \text{SP} \\ \text{PP} \\ \text{PS} \end{vmatrix}; \quad (7)$$

$$C_{\text{K1.3}} = \begin{pmatrix} 1 & 7 & 7 & 1 \\ 1/7 & 1 & 1 & 1/7 \\ 1/7 & 1 & 1 & 1/7 \\ 1 & 7 & 7 & 1 \end{pmatrix} \begin{vmatrix} \text{SS} \\ \text{SP} \\ \text{PP} \\ \text{PS} \end{vmatrix}; \quad (8)$$

 DOI: 10.26730/2618-7434-2026-3-4-25

$$C_{\text{K}1.4} = \begin{pmatrix} 1 & 9 & 9 & 1 \\ 1/9 & 1 & 1 & 1/9 \\ 1/9 & 1 & 1 & 1/9 \\ 1 & 9 & 9 & 1 \end{pmatrix} \begin{vmatrix} \text{SS} \\ \text{SP} \\ \text{PP} \\ \text{PS} \end{vmatrix}; \tag{9}$$

$$C_{\text{K}2.1} = \begin{pmatrix} 1 & 1/2 & 8 & 7 \\ 2 & 1 & 9 & 8 \\ 1/8 & 1/9 & 1 & 1/2 \\ 1/7 & 1/8 & 2 & 1 \end{pmatrix} \begin{vmatrix} \text{SS} \\ \text{SP} \\ \text{PP} \\ \text{PS} \end{vmatrix}; \tag{10}$$

$$C_{\text{K}2.3} = \begin{pmatrix} 1 & 1/3 & 7 & 5 \\ 3 & 1 & 9 & 7 \\ 1/7 & 1/9 & 1 & 1/3 \\ 1/5 & 1/7 & 3 & 1 \end{pmatrix} \begin{vmatrix} \text{SS} \\ \text{SP} \\ \text{PP} \\ \text{PS} \end{vmatrix}; \tag{11}$$

$$C_{\text{K}2.4} = \begin{pmatrix} 1 & 1/2 & 8 & 7 \\ 2 & 1 & 9 & 8 \\ 1/8 & 1/9 & 1 & 1/2 \\ 1/7 & 1/8 & 2 & 1 \end{pmatrix} \begin{vmatrix} \text{SS} \\ \text{SP} \\ \text{PP} \\ \text{PS} \end{vmatrix}. \tag{12}$$

All PCMs (5)-(12) are highly aligned. The consistency indices $k_{\text{CIK1.1}}$–$k_{\text{CIK2.4}}$ do not exceed 0.055 and the consistency ratios $k_{\text{CRK1.1}}$–$k_{\text{CRK2.4}}$ do not exceed 0.061, which indicates the correctness of the assessment made.

The eigenvectors for PCMs relating to second-level decision criteria $C_{Ki.j}$ are the local priorities vectors $V_{Ki.j}$. They are illustrated in Fig. 7, where the area of each figure indicates the preference of one or another compensation topology, provided that the first-level decision criteria are equally important.

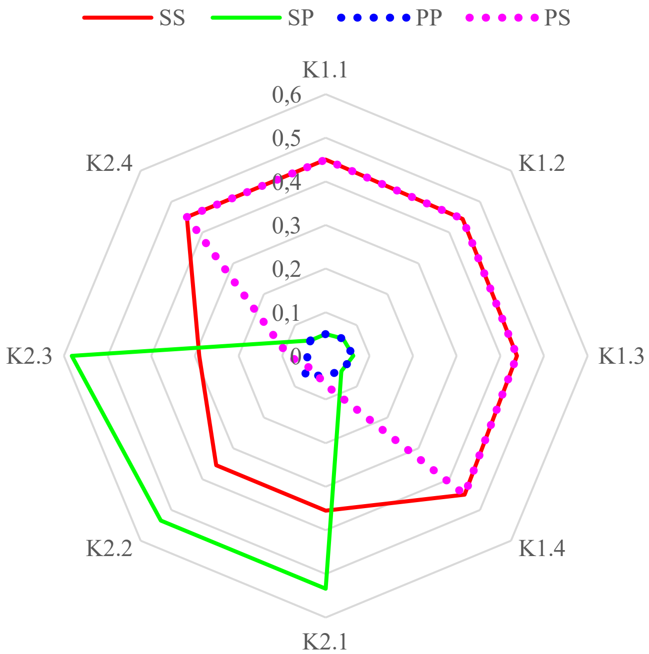

Fig. 7. Local priorities diagram
Рис. 7. Диаграмма локальных приоритетов

However, for real-life tasks, the first- and second-level decision criteria, as a rule, have different importance. To take this into account, the separate PCMs were compiled:

$$D_{\text{Ki}} = \begin{pmatrix} 1 & 1/3 \\ 3 & 1 \end{pmatrix} \begin{vmatrix} \text{K1} \\ \text{K2} \end{vmatrix};\qquad (13)$$

$$D_{\text{Ki.j}} = \begin{pmatrix} 1 & 2 & 9 & 7 \\ 1/2 & 1 & 9 & 5 \\ 1/9 & 1/9 & 1 & 1/2 \\ 1/7 & 1/5 & 2 & 1 \end{pmatrix} \begin{vmatrix} \text{Ki.1} \\ \text{Ki.2} \\ \text{Ki.3} \\ \text{Ki.4} \end{vmatrix},\qquad (14)$$

where for the first-level criteria it is assumed that A_U has a small priority over η, and for the second-level criteria the most important is normal conditions, and then in descending order of importance the changing of R_{load}, L_1 and M. The consistency indices k_{CIKi}, $k_{\text{CIKi.j}}$ do not exceed 0.02 and the consistency ratios k_{CRKi}, $k_{\text{CRKi.j}}$ do not exceed 0.023, which indicates the correctness of the matrix compilation.

The generalizing PCM of decision criteria is defined as the Kronecker product for (13) and (14):

$$D_K = D_{\text{Ki}} \otimes D_{\text{Ki.j}},\qquad (15)$$

and its eigenvector W_K is the relative importance vector. Then, by combining $V_{Ki.j}$ and taking W_K into account, the global priorities vector was determined:

$$G_R = V_K W_K = (V_{\text{K1.1}}, V_{\text{K1.2}}, V_{\text{K1.3}}, V_{\text{K1.4}}, V_{\text{K2.1}}, V_{\text{K2.2}}, V_{\text{K2.3}}, V_{\text{K2.4}}) W_K,\qquad (16)$$

which in the case under consideration is equal to:

$$G_R = \begin{pmatrix} 0.381 \\ 0.387 \\ 0.053 \\ 0.179 \end{pmatrix} \begin{vmatrix} \text{SS} \\ \text{SP} \\ \text{PP} \\ \text{PS} \end{vmatrix}.$$

Thus, under the considered conditions, the best compensation topology of DWCS for the underground suspended monorail is SP topology. At the same time, the small gap from SS topology that is the next preferable solution indicates the advisability of considering both of these options in the technical and economic assessment of real projects.

Conclusions

The analysis of energy-saving technologies for underground mining demonstrated the urgency of technological electric transport in this industry and the prospects for developing wireless charging systems for it. The conducted compensation topologies study of the dynamic wireless charging systems for the underground suspended monorail showed the following.

1. The efficiency η of wireless power transfer and the transmission ratio A_U depend significantly on the frequency and have a clearly expressed resonance at the frequency ω_r. The technically preferred value of η is demonstrated by SS and PS topologies, and the technically preferred value of A_U is so by SS and SP topologies.

2. For SS and PS topologies with an increase in R_{load} the value of η smoothly decreases but drops sharply in the vicinity of short-circuit, whereas for SP and PP topologies, an increase in R_{load} leads to a practically linear increase in η.

3. For SP and PP topologies an increase in R_{load} comes with a linear increase in A_U but for SS and PS topologies an increase in R_{load} comes with an exponential saturation of A_U. It is notable that in the vicinity of normal conditions, the value of A_U for PS becomes virtually constant.

4. An increase in M leads to an increase in η for all topologies, but for the SS and PS topologies, this increase is of exponential saturation nature. For PS and PP topologies, an increase in M leads to an increase in A_U, and for SS and SP topologies, the trend is the opposite because of bifurcation. Remarkably for SS and SP topologies the value of A_U even reduced due to bifurcation is significantly higher than for PS and PP topologies.

5. For all topologies, both η and A_U show an inverse dependence on L_1, which indicates the limit existed for the rational length of the transmitting line. This means that the dynamic wireless charging system with a high working length requires sectioning of the transmitting equipment.

The obtained equations for the performance indicators of the dynamic wireless charging system can be used to select specific parameters of DWCS for a specific object, for example, to optimize parameters under given constraints. The proposed approach to the comparative analysis of compensation topologies can be useful in substantiating technical solutions in real projects for implementing dynamic wireless charging systems for technological electric transport. Combining the analytic hierarchy process with the expert survey method might be recommended for a more accurate comparative analysis.

APPENDIX

This section presents the derivation of the equations from Table 1 relating η and A_U to the parameters of the dynamic wireless charging system including R_{load}, L_1, and M. The derivation is carried out sequentially for each of the topologies considered in the article.

A. *SS topology*

Fig. 2a shows the idealized equivalent circuits of DWCS with SS topology, according to which the mathematical model in the time domain in the form of differential equations is:

$$\begin{gathered} u_1 = u_{C1} + i_1 R_1 + L_1 \frac{di_1}{dt} + M\frac{di_2}{dt}; \\ 0 = u_{C2} + i_2 R_2 + i_2 R_{load} + L_2 \frac{di_2}{dt} + M\frac{di_1}{dt}; \\ i_1 = C_1 \frac{du_{C1}}{dt}; \\ i_2 = C_2 \frac{du_{C2}}{dt}; \\ u_2 = i_2 R_{load}, \end{gathered} \tag{A1}$$

From here, to use the transfer functions tool with the Laplace transform we obtain the mathematical model in operator form:

$$\begin{aligned} &U_1 = U_{C1} + I_1 R_1 + sI_1 L_1 + sI_2 M; \\ &0 = U_{C2} + I_2(R_2 + R_{load}) + sI_2 L_2 + sI_1 M; \\ &I_1 = sU_{C1}C_1; \\ &I_2 = sU_{C2}C_2. \end{aligned} \tag{A2}$$

After that, the equation (1) becomes the following:

$$\eta = \frac{|I_2|^2 R_{load}}{|I_1|^2\, Re(Z_{in})}, \tag{A3}$$

where Z_{in} is the input impedance, and equation (2) is respectively:

$$A_U = \frac{|I_2| R_{load}}{|U_1|}. \tag{A4}$$

Let us use the following transfer functions:

$$W_{i_{2SS}}(s) = \frac{I_2(s)}{U_1(s)} = \frac{s^3 a_{1SS}}{s^4 b_{1SS} + s^3 b_{2SS} + s^2 b_{3SS} + s b_{4SS} + 1}; \tag{A5}$$

$$W_{i_{1SS}}(s) = \frac{I_1(s)}{U_1(s)} = \frac{(s^3 a_{2SS} + s^2 a_{3SS} + s) a_{4SS}}{s^4 b_{1SS} + s^3 b_{2SS} + s^2 b_{3SS} + s b_{4SS} + 1}, \tag{A6}$$

where:

$$a_{1ss} = -MC_1C_2; \quad b_{1ss} = (L_1L_2 - M^2)C_1C_2;$$
$$a_{2ss} = L_2C_2; \quad b_{2ss} = (R_1L_2 + (R_2 + R_{load})L_1)C_1C_2;$$
$$a_{3ss} = (R_2 + R_{load})C_2; \quad b_{3ss} = R_1(R_2 + R_{load})C_1C_2 + L_1C_1 + L_2C_2;$$
$$a_{4ss} = C_1; \quad b_{4ss} = R_1C_1 + (R_2 + R_{load})C_2,$$

that in the frequency domain rewrite as:

$$W_{i_{2ss}}(j\omega) = \frac{I_2(j\omega)}{U_1(j\omega)} = Re(W_{i_{2ss}}) + j\,Im(W_{i_{2ss}}) = A_{i_{2ss}}(\omega)e^{j\varphi_{i_{2ss}}(\omega)}; \quad \text{(A7)}$$

$$W_{i_{1ss}}(j\omega) = \frac{I_1(j\omega)}{U_1(j\omega)} = Re(W_{i_{1ss}}) + j\,Im(W_{i_{1ss}}) = A_{i_{1ss}}(\omega)e^{j\varphi_{i_{1ss}}(\omega)}. \quad \text{(A8)}$$

Taking $U_1(j\omega)=|U_1|e^{j0}$ we carry out the following calculations:

$$P_{load} = |I_2|^2R_{load} = |U_1|^2A^2_{i_{2ss}}R_{load}; \quad \text{(A9)}$$

$$P_{in} = |I_1|^2\,Re(Z_{in}) = |U_1||I_1|\cos(\varphi_{i_{1ss}}) = |U_1|^2\,Re(W_{i_{1ss}}). \quad \text{(A10)}$$

Thus:

$$\eta = \frac{|U_1|^2A^2_{i_{2ss}}R_{load}}{|U_1|^2\,Re(W_{i_{1ss}})} = \frac{A^2_{i_{2ss}}R_{load}}{Re(W_{i_{1ss}})}; \quad \text{(A11)}$$

$$A_U = \frac{|U_1|A_{i_{2ss}}R_{load}}{|U_1|} = A_{i_{2ss}}R_{load}. \quad \text{(A12)}$$

B. *SP topology*

Fig. 2b shows the idealized equivalent circuits of DWCS with SP topology, according to which the mathematical model in the time domain in the form of differential equations is:

$$\begin{aligned}
u_1 &= u_{C1} + i_1R_1 + L_1\frac{di_1}{dt} + M\frac{di_2}{dt};\\
0 &= u_{C2} + i_2R_2 + L_2\frac{di_2}{dt} + M\frac{di_1}{dt};\\
i_1 &= C_1\frac{du_{C1}}{dt};\\
i_{C2} &= C_2\frac{du_{C2}}{dt};\\
i_2 &= i_{C2} + i_{load};\\
u_2 &= u_{C2} = i_2R_{load},
\end{aligned} \quad \text{(A13)}$$

from here the mathematical model in operator form:

$$\begin{aligned}
U_1 &= U_{C1} + I_1R_1 + sI_1L_1 + sI_2M;\\
0 &= U_{C2} + I_2R_2 + sI_2L_2 + sI_1M;\\
I_1 &= sU_{C1}C_1;\\
I_{C2} &= sU_{C2}C_2;\\
I_2 &= I_{C2} + I_{load};\\
U_{C2} &= I_{load}R_{load}.
\end{aligned} \quad \text{(A14)}$$

The equation (1) becomes the following:

$$\eta = \frac{|I_{load}|^2R_{load}}{|I_1|^2\,Re(Z_{in})}, \quad \text{(A15)}$$

and equation (2) is respectively:

$$A_U = \frac{|I_{load}|R_{load}}{|U_1|}. \quad \text{(A16)}$$

Let us use the following transfer functions:

$$W_{i_{load\ sp}}(s)=\frac{I_{load}(s)}{U_1(s)}=\frac{s^2a_{1sp}}{s^4b_{1sp}+s^3b_{2sp}+s^2b_{3sp}+sb_{4sp}+b_{5sp}};\quad (A17)$$

$$W_{i_{1sp}}(s)=\frac{I_1(s)}{U_1(s)}=\frac{s^3a_{2sp}+s^2a_{3sp}+sa_{4sp}}{s^4b_{1sp}+s^3b_{2sp}+s^2b_{3sp}+sb_{4sp}+b_{5sp}},\quad (A18)$$

where:

$a_{1sp}=MC_1;$
$a_{2sp}=R_{load}L_2C_1C_2;$
$a_{3sp}=(R_2R_{load}C_2+L_2)C_1;$
$a_{4sp}=(R_2+R_{load})C_1;$

$b_{1sp}=R_{load}(L_1L_2-M^2)C_1C_2;$
$b_{2sp}=R_{load}(R_2L_1+R_1L_2)C_1C_2+(L_1L_2-M^2)C_1;$
$b_{3sp}=(R_2+R_{load})L_1C_1+R_{load}L_2C_2+R_1L_2C_1+R_1R_2R_{load}C_1C_2;$
$b_{4sp}=R_1(R_2+R_{load})C_1+R_2R_{load}C_2+L_2;$
$b_{5sp}=R_2+R_{load},$

that in the frequency domain rewrite as:

$$W_{i_{load\ sp}}(j\omega)=\frac{I_{load}(j\omega)}{U_1(j\omega)}=Re(W_{i_{load\ sp}})+j\,Im(W_{i_{load\ sp}})=A_{i_{load\ sp}}(\omega)e^{j\varphi_{i_{load\ sp}}(\omega)};\quad (A19)$$

$$W_{i_{1sp}}(j\omega)=\frac{I_1(j\omega)}{U_1(j\omega)}=Re(W_{i_{1sp}})+j\,Im(W_{i_{1sp}})=A_{i_{1sp}}(\omega)e^{j\varphi_{i_{1sp}}(\omega)}.\quad (A20)$$

Taking $U_1(j\omega)=|U_1|e^{j0}$ we carry out the following calculations:

$$P_{load}=|I_{load}|^2R_{load}=|U_1|^2A^2_{i_{load\ sp}}R_{load};\quad (A21)$$

$$P_{in}=|I_1|^2\,Re(Z_{in})=|U_1||I_1|\cos(\varphi_{i_{1sp}})=|U_1|^2\,Re(W_{i_{1sp}}).\quad (A22)$$

Thus:

$$\eta=\frac{|U_1|^2A^2_{i_{load\ sp}}R_{load}}{|U_1|^2\,Re(W_{i_{1sp}})}=\frac{A^2_{i_{load\ sp}}R_{load}}{Re(W_{i_{1sp}})};\quad (A23)$$

$$A_U=\frac{|U_1|A_{i_{load\ sp}}R_{load}}{|U_1|}=A_{i_{load\ sp}}R_{load}.\quad (A24)$$

C. *PP topology*

Figure 2d shows the idealized equivalent circuits of DWCS with PP topology, according to which the mathematical model in the time domain in the form of differential equations is:

$$\begin{aligned}
&u_{C1}=i_1R_1+L_1\frac{di_1}{dt}+M\frac{di_2}{dt};\\
&0=u_{C2}+i_2R_2+L_2\frac{di_2}{dt}+M\frac{di_1}{dt};\\
&i_{C1}=C_1\frac{du_{C1}}{dt};\\
&i_{C2}=C_2\frac{du_{C2}}{dt};\\
&i_{in}=i_{C1}+i_1;\\
&i_2=i_{C2}+i_{load};\\
&u_1=u_{C1};\\
&u_2=u_{C2}=i_{load}R_{load},
\end{aligned}\quad (A25)$$

from here the mathematical model in operator form:

 DOI: 10.26730/2618-7434-2026-3-4-25

$$\begin{aligned}&U_{C1} = I_1R_1 + sI_1L_1 + sI_2M;\\&0 = U_{C2} + I_2R_2 + sI_2L_2 + sI_1M;\\&I_{C1} = sU_{C1}C_1;\\&I_{C2} = sU_{C2}C_2;\\&I_{in} = I_{C1} + I_1;\\&I_2 = I_{C2} + I_{load};\\&U_{C2} = I_{load}R_{load}.\end{aligned} \quad (A26)$$

The equation (1) becomes the following:

$$\eta = \frac{|I_{load}|^2 R_{load}}{|I_{in}|^2\, Re(Z_{in})}, \quad (A27)$$

and equation (2) is respectively:

$$A_U = \frac{|I_{load}| R_{load}}{|U_{C1}|}. \quad (A28)$$

Let us use the following transfer functions:

$$W_{i_{load\ pp}}(s) = \frac{I_{load}(s)}{I_{in}(s)} = \frac{sa_{1pp}}{s^4 b_{1pp} + s^3 b_{2pp} + s^2 b_{3pp} + s b_{4pp} + b_{5pp}}; \quad (A29)$$

$$W_{u_{C1pp}}(s) = \frac{U_{C1}(s)}{I_{in}(s)} = \frac{s^3 a_{2pp} + s^2 a_{3pp} + s a_{4pp} + a_{5pp}}{s^4 b_{1pp} + s^3 b_{2pp} + s^2 b_{3pp} + s b_{4pp} + b_{5pp}}, \quad (A30)$$

where:

$a_{1pp} = -M$; $b_{1pp} = R_{load}(L_1L_2 - M^2)C_1C_2$;
$a_{2pp} = R_{load}(L_1L_2 - M^2)C_2$; $b_{2pp} = R_{load}(R_1L_2 + R_2L_1)C_1C_2 + (L_1L_2 - M^2)C_1$;
$a_{3pp} = (L_2L_1 - M^2) + R_{load}(R_1L_2 + R_2L_1)C_2$; $b_{3pp} = R_1R_2R_{load}C_1C_2 + R_{load}(L_2C_2 + L_1C_1) + (R_1L_2 + R_2L_1)C_1$;
$a_{4pp} = R_1L_2 + R_2L_1 + R_{load}(R_1R_2C_2 + L_1)$; $b_{4pp} = R_1(R_2 + R_{load})C_1 + R_2R_{load}C_2 + L_2$;
$a_{5pp} = R_1(R_2 + R_{load})$; $b_{5pp} = R_2 + R_{load}$,

that in the frequency domain rewrite as:

$$W_{i_{load\ pp}}(j\omega) = \frac{I_{load}(j\omega)}{I_{in}(j\omega)} = Re(W_{i_{load\ pp}}) + j\,Im(W_{i_{load\ pp}}) = A_{i_{load\ pp}}(\omega)e^{j\varphi_{i_{load\ pp}}(\omega)}; \quad (A31)$$

$$W_{u_{C1pp}}(j\omega) = \frac{U_{C1}(j\omega)}{I_{in}(j\omega)} = Re(W_{u_{C1pp}}) + j\,Im(W_{u_{C1pp}}) = A_{u_{C1pp}}(\omega)e^{j\varphi_{u_{C1pp}}(\omega)}. \quad (A32)$$

Considering that U_{C1}/I_{in} is the input impedance of the wireless charging system we carry out the following calculations:

$$P_{load} = |I_{load}|^2 R_{load} = |I_{in}|^2 A^2_{i_{load\ pp}} R_{load}; \quad (A33)$$

$$P_{in} = |I_{in}|^2\, Re(Z_{in}) = |I_{in}|^2\, Re(W_{u_{C1pp}}). \quad (A34)$$

Thus:

$$\eta = \frac{|I_{in}|^2 A^2_{i_{load\ pp}} R_{load}}{|I_{in}|^2\, Re(W_{u_{C1pp}})} = \frac{A^2_{i_{load\ pp}} R_{load}}{Re(W_{u_{C1pp}})}; \quad (A35)$$

$$A_U = \frac{|I_{load}| R_{load}}{|U_{C1}|} = \frac{|I_{in}| A_{i_{load\ pp}} R_{load}}{|I_{in}| A_{u_{C1pp}}} = \frac{A_{i_{load\ pp}} R_{load}}{A_{u_{C1pp}}}. \quad (A36)$$

D. *PS topology*

Fig. 2c shows the idealized equivalent circuits of DWCS with PS topology, according to which the mathematical model in the time domain in the form of differential equations is:

DOI: 10.26730/2618-7434-2026-3-4-25

$$\begin{aligned} &u_{C1} = i_1 R_1 + L_1 \frac{di_1}{dt} + M \frac{di_2}{dt}; \\ &0 = u_{C2} + i_2 R_2 + i_2 R_{load} + L_2 \frac{di_2}{dt} + M \frac{di_1}{dt}; \\ &i_{C1} = C_1 \frac{du_{C1}}{dt}; \\ &i_2 = C_2 \frac{du_{C2}}{dt}; \\ &i_{in} = i_{C1} + i_1; \\ &u_1 = u_{C1}; \\ &u_2 = i_2 R_{load}, \end{aligned} \quad \text{(A37)}$$

from here the mathematical model in operator form:

$$\begin{aligned} &U_{C1} = I_1 R_1 + sI_1 L_1 + sI_2 M; \\ &0 = U_{C2} + I_2 R_2 + I_2 R_{load} + sI_2 L_2 + sI_1 M; \\ &I_{C1} = sU_{C1} C_1; \\ &I_2 = sU_{C2} C_2; \\ &I_{in} = I_{C1} + I_1; \\ &U_2 = I_2 R_{load}. \end{aligned} \quad \text{(A38)}$$

The equation (1) becomes the following:

$$\eta = \frac{|I_2|^2 R_{load}}{|I_{in}|^2\, Re(Z_{in})}, \quad \text{(A39)}$$

and equation (2) is respectively:

$$A_U = \frac{|I_2| R_{load}}{|U_{C1}|}. \quad \text{(A40)}$$

Let us use the following transfer functions:

$$W_{i_2\,ps}(s) = \frac{I_2(s)}{I_{in}(s)} = \frac{s^2 a_{1ps}}{s^4 b_{1ps} + s^3 b_{2ps} + s^2 b_{3ps} + s b_{4ps} + 1}; \quad \text{(A41)}$$

$$W_{u_{C1ps}}(s) = \frac{U_{C1}(s)}{I_{in}(s)} = \frac{s^3 a_{2ps} + s^2 a_{3ps} + s a_{4ps} + a_{5ps}}{s^4 b_{1ps} + s^3 b_{2ps} + s^2 b_{3ps} + s b_{4ps} + 1}, \quad \text{(A42)}$$

where:

$$\begin{aligned} &a_{1ps} = -MC_2; \\ &a_{2ps} = (L_1 L_2 - M^2) C_2; \\ &a_{3ps} = (R_1 L_2 + (R_2 + R_{load}) L_1) C_2; \\ &a_{4ps} = R_1 (R_2 + R_{load}) C_1 + L_1; \\ &a_{5ps} = R_1; \end{aligned} \qquad \begin{aligned} &b_{1ps} = (L_1 L_2 - M^2) C_1 C_2; \\ &b_{2ps} = (R_1 L_2 + (R_2 + R_{load}) L_1) C_1 C_2; \\ &b_{3ps} = L_1 C_1 + L_2 C_2 + R_1 (R_2 + R_{load}) C_1 C_2; \\ &b_{4ps} = R_1 C_1 + (R_2 + R_{load}) C_2, \end{aligned}$$

that in the frequency domain rewrite as:

$$W_{i_{2ps}}(j\omega) = \frac{I_2(j\omega)}{I_{in}(j\omega)} = Re(W_{i_{2ps}}) + j\, Im(W_{i_{2ps}}) = A_{i_{2ps}}(\omega) e^{j\varphi_{i_{2ps}}(\omega)}; \quad \text{(A43)}$$

$$W_{u_{C1ps}}(j\omega) = \frac{U_{C1}(j\omega)}{I_{in}(j\omega)} = Re(W_{u_{C1ps}}) + j\, Im(W_{u_{C1ps}}) = A_{u_{C1ps}}(\omega) e^{j\varphi_{u_{C1ps}}(\omega)}. \quad \text{(A44)}$$

Considering that U_{C1}/I_{in} is the input impedance of the wireless charging system we carry out the following calculations:

$$P_{load} = |I_2|^2 R_{load} = |I_{in}|^2 A_{i_{2ps}}^2 R_{load}; \tag{A45}$$

$$P_{in} = |I_{in}|^2\, Re(Z_{in}) = |I_{in}|^2\, Re(W_{u_{C1ps}}). \tag{A46}$$

Thus:

$$\eta = \frac{|I_{in}|^2 A_{i_{2ps}}^2 R_{load}}{|I_{in}|^2\, Re(W_{u_{C1ps}})} = \frac{A_{i_{2ps}}^2 R_{load}}{Re(W_{u_{C1ps}})}; \tag{A47}$$

$$A_U = \frac{|I_2| R_{load}}{|U_{C1}|} = \frac{|I_{in}| A_{i_{2ps}} R_{load}}{|I_{in}| A_{u_{C1ps}}} = \frac{A_{i_{2ps}} R_{load}}{A_{u_{C1ps}}}. \tag{A48}$$

Conflicts of Interest

The authors declare no conflict of interest.

© 2026 The Authors. Published by T. F. Gorbachev Kuzbass State Technical University. This is an open access article under the CC BY license (http://creativecommons.org/licenses/by/4.0/).

Information about the authors

Valery M. Zavyalov, Dr.Sc. (Eng.), Professor, Department of Electric Energy
e-mail: VMZavyalov@sevsu.ru

Sergey A. Abeidulin, Senior Lecturer, Department of Electric Energy
e-mail: SAAbeidulin@sevsu.ru

Nikolay M. Shaitor, PhD (Eng.), Associate Professor, Department of Electric Energy
e-mail: shaytor1950@mail.ru

Sevastopol State University, 33 Universitetskaya str., Sevastopol, 299053, Russian Federation

Irina Yu. Semykina, Dr.Sc. (Eng.), Senior Researcher, Mining Industry Digital Transformation Laboratory
e-mail: semykinaiju@kuzstu.ru

Gennady M. Lebedev, Dr. Sc. (Engineering), Professor, Professor of the Department of Electrical Supply of Mining and Industrial Enterprises
e-mail: lgm.egpp@kuzstu.ru

T.F. Gorbachev Kuzbass State Technical University, 28 Vesennaya St., Kemerovo, 650000, Russian Federation

References

1. Weilong Wang, Xiaodong Yang, Jianhong Cao, Wenchao Bu, Abd Alwahed Dagestani, Tomiwa Sunday Adebayo, Azer Dilanchiev, Siyu Ren. Energy internet, digital economy, and green economic growth: Evidence from China. *Innovation and Green Development.* 2022;1(2):1-12. DOI: 10.1016/j.igd.2022.100011
2. Bijan Bibak, Hatice Tekiner-Mogulkoc. Influences of vehicle to grid (V2G) on power grid: An analysis by considering associated stochastic parameters explicitly. *Sustainable Energy, Grids and Networks.* 2021;26:100429. DOI: 10.1016/j.segan.2020.100429.
3. Rebecca Gough, Charles Dickerson, Paul Rowley, Chris Walsh. Vehicle-to-grid feasibility: A techno-economic analysis of EV-based energy storage. *Applied Energy.* 2017;192:12-23. DOI: 10.1016/j.apenergy.2017.01.102.
4. Laiqing Xie, Yugong Luo, Donghao Zhang, Rui Chen, Keqiang Li. Intelligent energy-saving control strategy for electric vehicle based on preceding vehicle movement. *Mechanical Systems and Signal Processing.* 2019;130:484-501. DOI: 10.1016/j.ymssp.2019.05.027.
5. Alessandro Augello, Pierluigi Gallo, Eleonora Riva Sanseverino, Gaetano Sciabica, Giuseppe Sciumè. Certifying battery usage for V2G and second life with a blockchain-based framework. *Computer Networks.* 2023;222:109558. DOI: 10.1016/j.comnet.2023.109558.

6. Muhammad Shahid Mastoi, Shenxian Zhuang, Hafiz Mudassir Munir, Malik Haris, Mannan Hassan, Muhammad Usman, Syed Sabir Hussain Bukhari, Jong-Suk Ro. An in-depth analysis of electric vehicle charging station infrastructure, policy implications, and future trends. *Energy Reports.* 2022;8:11504-11529. DOI: 10.1016/j.egyr.2022.09.011.
7. Sadeq Ali Qasem Mohammed, Jin-Woo Jung. A Comprehensive State-of-the-Art Review of Wired/Wireless Charging Technologies for Battery Electric Vehicles: Classification/Common Topologies/Future Research Issues. *IEEE Access.* 2021;9:19572-19585. DOI: 10.1109/ACCESS.2021.3055027.
8. Brenna M., Foiadelli F., Leone C., Longo M. Electric Vehicles Charging Technology Review and Optimal Size Estimation. *Journal of Electrical Engineering & Technology.* 2020;15:2539-2552. DOI: 10.1007/s42835-020-00547-x.
9. Khaligh A., D'Antonio M. Global Trends in High-Power On-Board Chargers for Electric Vehicles. *IEEE Transactions on Vehicular Technology.* 2019;68(4):3306-3324. DOI: 10.1109/TVT.2019.2897050.
10. Vincenzo Cirimele, Michela Diana, Fabio Freschi, Massimo Mitolo. Inductive Power Transfer for Automotive Applications: State-of-the-Art and Future Trends. *IEEE Transactions on Industry Applications.* 2018;54(5):4069-4079. DOI: 10.1109/TIA.2018.2836098.
11. Jian-guo Li, Kai Zhan. Intelligent Mining Technology for an Underground Metal Mine Based on Unmanned Equipment. *Engineering.* 2018;4(3):381-391. DOI: 10.1016/j.eng.2018.05.013.
12. Jäderblom N. From Diesel to Battery Power in Underground Mines. A Pilot Study of Diesel Free LHDs: M.Sc. Thesis in Industrial Design Engineering. Luleå: Luleå University of Technology, 2017. 75 p.
13. Shirin L.N., Rastsvetaev V.A., Koval A.I. Improving the efficiency of monorail roads when preparing coal reserves for extraction. Donetsk: NSU, 2014. 144 p. [In Russ.].
14. Ryabko K.A., Gutarevich V.O., Ryabko E.V., Kondratenko M.P. Rolling stock of a mine suspended monorail. Patent RU 2770968 C1, IPC E21F 13/00. No. 2021122860: declared 07/29/2021: published 04/25/2022. [In Russ.].
15. Saleem Khawaja. Efficient suspended monorail locomotive transportation systems for underground mines // MiningTechnology, January 12, 2023. URL: https://www.mining-technology.com/sponsored/suspended-mining-locomotive-ferrit-dlz130f/
16. Klontz K. W., Divan D. M., Novotny D. W., Lorenz R. D. Contactless Power Delivery System for Mining Applications. *IEEE Transactions on Industry Applications.* 1995;31(1):27-35. DOI: 10.1109/28.363053.
17. Manual. Contactless Energy Transfer System. MOVITRANS® line Transfer System for TDM90E Flat Pickups. Project Planning. 31559441/EN, Jan. 2024. URL: https://download.sew-eurodrive.com/download/pdf/31559441.pdf#search=%22PLAA;PLA;PL;P%22
18. Costa V. S., Marques E., Mendes A. M., Perdigão M. S. Resonant converter topology impact on a Dynamic IPT application // 2021 Telecoms Conference (ConfTELE). IEEE, 2021. pp. 1-6.
19. Fujita T., Yasuda T., Akagi H. A Dynamic Wireless Power Transfer System Applicable to a Stationary System. *IEEE Transactions on Industry Applications.* 2017;53(4):3748-3757. DOI: 10.1109/TIA.2017.2680400.
20. Guo Y., Wang L., Zhu Q., Liao C., Li F. Switch-On Modeling and Analysis of Dynamic Wireless Charging System Used for Electric Vehicles. *IEEE Transactions on Industrial Electronics.* 2016;63(10):6568-6579. DOI: 10.1109/TIE.2016.2557302.
21. Zeng Rong, Onar Omer, Mohammad Mostak, Su Gui-Jia, Asa Erdem, Galigekere Veda Prakash. Modeling and Analysis of a Polyphase Wireless Power Transfer System for EV Charging Applications. *In: IEEE Applied Power Electronics Conference and Exposition (APEC).* IEEE, 2022. pp. 1871097. DOI: 10.1109/APEC43599.2022.9773533.
22. Foote A., Onar O. C. A review of high-power wireless power transfer. *In: 2017 IEEE Transportation Electrification Conference and Expo (ITEC)*. IEEE, 2017. pp. 234-240.
23. Esteban B., Sid-Ahmed M., Kar N. C. A comparative study of power supply architectures in wireless EV charging systems. *IEEE Transactions on Power Electronics.* 2015;30(11):6408-6422.
24. Shevchenko V., Husev O., Strzelecki R., Pakhaliuk B., Poliakov N., Strzelecka N. Compensation topologies in IPT systems: Standards, requirements, classification, analysis, comparison and application. *IEEE Access.* 2019;7:120559-120580.
25. Zhang W., Mi C. C. Compensation topologies of high-power wireless power transfer systems. *IEEE Transactions on Vehicular Technology.* 2015;65(6):4768-4778.
26. Mude K. N., Aditya K. Comprehensive review and analysis of two-element resonant compensation topologies for wireless inductive power transfer systems. *Chinese Journal of Electrical Engineering.* 2019;5(2):14-31.
27. Xiaohui Qu, Hongdou Han, Siu-Chung Wong, Chi K. Tse, Wu Chen. Hybrid IPT topologies with constant current or constant voltage output for battery charging applications. *IEEE Transactions on Power Electronics.* 2015;30(11):6329-6337.

28. Shuyu Cao, Htet Ye Yint Naing, R.T. Naayagi, Sze Sing Lee, Feng Wei, King Jet Tseng. Wireless charging resonant converter topology study based on analytical design computation. *In: 2020 3rd International Conference on Energy, Power and Environment: Towards Clean Energy Technologies*. IEEE, 2021. pp. 1-6.
29. Aditya K., Williamson S. S. Design guidelines to avoid bifurcation in a series–series compensated inductive power transfer system. *IEEE Transactions on Industrial Electronics.* 2018;66(5):3973-3982.
30. Wang B., Hu A. P., Budgett D. Maintaining middle zero voltage switching operation of parallel–parallel tuned wireless power transfer system under bifurcation. *IET Power Electronics.* 2014;7(1):78-84.
31. Matteo Brunelli. Introduction to the Analytic Hierarchy Process. Springer Cham, 2015. 83 p. DOI: 10.1007/978-3-319-12502-2.
32. Algafri M., Alghazi A., Almoghathawi Y., Saleh H., Al-Shareef K. Smart City Charging Station Allocation for Electric Vehicles Using Analytic Hierarchy Process and Multiobjective Goal-programming. *Applied Energy.* 2024;372:123775. DOI: 10.1016/j.apenergy.2024.123775.

УДК 621.354

ИССЛЕДОВАНИЕ КОМПЕНСАЦИОННЫХ ТОПОЛОГИЙ ДИНАМИЧЕСКОЙ СИСТЕМЫ БЕСПРОВОДНОГО ЗАРЯДА ДЛЯ ПОДЗЕМНОЙ ПОДВЕСНОЙ МОНОРЕЛЬСОВОЙ ДОРОГИ

Завьялов В.М.[1,2], Семыкина И.Ю.[2], Абейдулин С.А.[1], Шайтор Н.М.[1], Лебедев Г.М.[2]

[1] Севастопольский государственный университет
[2] Кузбасский государственный технический университет им. Т.Ф. Горбачева

CC BY

Информация о статье
Поступила:
11 марта 2026 г.

Рецензирование:
02 июня 2026 г.

Принята к печати:
03 июля 2026 г.

Ключевые слова:
электромобиль, подземная подвесная монорельсовая дорога, динамическая система беспроводного зарядка, беспроводная передача энергии, компенсационная топология, аккумуляторная батарея, эквивалентная нагрузка, передающая линия, КПД, передаточная функция, метод анализа иерархий

Аннотация.
Внедрение электрических транспортных средств и создание соответствующей зарядной инфраструктуры активно развиваются, включая их использование в промышленной сфере. Подземная подвесная монорельсовая дорога — разновидность горного рельсового транспорта, в которой отмечается тенденция к использованию локомотивов с электроприводом, питающимся от аккумуляторных батарей. Одним из перспективных методов их зарядки является применение динамической системы беспроводного заряда, основанной на использовании длинной линии на стороне передатчика. Для таких систем влияние топологии компенсационных цепей на качество работы изучено недостаточно. В статье исследуются четыре двухэлементные топологии. В качестве показателей эффективности выбраны: эффективность беспроводной передачи энергии и коэффициент передачи, который показывает отношение выходного напряжения резонансного контура, указывающего на напряжение нагрузки, к входному напряжению резонансного контура. Для каждой топологии составлена математическая модель и получены параметрические уравнения, описывающие показатели эффективности. Проведен анализ показателей эффективности динамической системы беспроводного заряда с различными компенсационными топологиями с учетом особенностей подземной подвесной монорельсовой дороги. На основе полученных результатов с использованием метода аналитической иерархии выбрана наилучшая топология для рассматриваемых условий.

Для цитирования: Завьялов В.М., Семыкина И.Ю., Абейдулин С.А., Шайтор Н.М., Лебедев Г.М/ Исследование компенсационных топологий динамической системы беспроводного заряда для подземной подвесной монорельсовой дороги // Техника и технология горного дела. – 2026. – №3(34). – С. 4-25. – DOI:10.26730/2618-7434-2026-3-4-25, EDN: HKQZIL

Благодарность: исследование выполнено при финансовой поддержке государственного задания Министерства науки и высшего образования Российской Федерации (№ 075-03-2024-082-2).

Список литературы

1. Weilong Wang, Xiaodong Yang, Jianhong Cao, Wenchao Bu, Abd Alwahed Dagestani, Tomiwa Sunday Adebayo, Azer Dilanchiev, Siyu Ren. Energy internet, digital economy, and green economic growth: Evidence from China // Innovation and Green Development. – 2022. – Vol. 1. – Iss. 2. – pp. 1-12. DOI: 10.1016/j.igd.2022.100011.
2. Bijan Bibak, Hatice Tekiner-Mogulkoc. Influences of vehicle to grid (V2G) on power grid: An analysis by considering associated stochastic parameters explicitly // Sustainable Energy, Grids and Networks. – 2021. – Vol. 26. – pp. 100429. DOI: 10.1016/j.segan.2020.100429.
3. Rebecca Gough, Charles Dickerson, Paul Rowley, Chris Walsh. Vehicle-to-grid feasibility: A techno-economic analysis of EV-based energy storage // Applied Energy. – 2017. – Vol. 192. – pp. 12-23. DOI: 10.1016/j.apenergy.2017.01.102.
4. Laiqing Xie, Yugong Luo, Donghao Zhang, Rui Chen, Keqiang Li. Intelligent energy-saving control strategy for electric vehicle based on preceding vehicle movement // Mechanical Systems and Signal Processing. – 2019. – Vol. 130. – pp. 484-501. DOI: 10.1016/j.ymssp.2019.05.027.
5. Alessandro Augello, Pierluigi Gallo, Eleonora Riva Sanseverino, Gaetano Sciabica, Giuseppe Sciumè. Certifying battery usage for V2G and second life with a blockchain-based framework // Computer Networks. – 2023. – Vol. 222. – pp. 109558. DOI: 10.1016/j.comnet.2023.109558.
6. Muhammad Shahid Mastoi, Shenxian Zhuang, Hafiz Mudassir Munir, Malik Haris, Mannan Hassan, Muhammad Usman, Syed Sabir Hussain Bukhari, Jong-Suk Ro. An in-depth analysis of electric vehicle charging station infrastructure, policy implications, and future trends // Energy Reports. – 2022. – Vol. 8. – pp. 11504-11529. DOI: 10.1016/j.egyr.2022.09.011.
7. Sadeq Ali Qasem Mohammed, Jin-Woo Jung. A Comprehensive State-of-the-Art Review of Wired/Wireless Charging Technologies for Battery Electric Vehicles: Classification/Common Topologies/Future Research Issues // IEEE Access. – 2021. – Vol. 9. – pp. 19572-19585. DOI: 10.1109/ACCESS.2021.3055027.
8. Brenna M., Foiadelli F., Leone C., Longo M. Electric Vehicles Charging Technology Review and Optimal Size Estimation // Journal of Electrical Engineering & Technology. – 2020. – Vol. 15. – pp. 2539-2552. DOI: 10.1007/s42835-020-00547-x.
9. Khaligh A., D'Antonio M. Global Trends in High-Power On-Board Chargers for Electric Vehicles // IEEE Transactions on Vehicular Technology. – 2019. – Vol. 68. – No. 4. – pp. 3306-3324. DOI: 10.1109/TVT.2019.2897050.
10. Vincenzo Cirimele, Michela Diana, Fabio Freschi, Massimo Mitolo. Inductive Power Transfer for Automotive Applications: State-of-the-Art and Future Trends // IEEE Transactions on Industry Applications. – 2018. – Vol. 54. – No. 5. – pp. 4069-4079. DOI: 10.1109/TIA.2018.2836098.
11. Jian-guo Li, Kai Zhan. Intelligent Mining Technology for an Underground Metal Mine Based on Unmanned Equipment // Engineering. – 2018. – Vol. 4. – Iss. 3. – pp. 381-391. DOI: 10.1016/j.eng.2018.05.013.
12. Jäderblom N. From Diesel to Battery Power in Underground Mines. A Pilot Study of Diesel Free LHDs: Master of Science Thesis in Industrial Design Engineering. Luleå: Luleå University of Technology, 2017. 75 p.
13. Ширин Л.Н., Расцветаев В.А., Коваль А.И. Повышение эффективности работы монорельсовых дорог при подготовке запасов угля к очистной выемке: монография. Днепропетровск: НГУ, 2014. 144 с.
14. Патент № 2770968 C1 Российская Федерация, МПК E21F 13/00. Подвижной состав шахтной подвесной монорельсовой дороги: № 2021122860: заявл. 29.07.2021: опубл. 25.04.2022 / К. А. Рябко, В. О. Гутаревич, Е. В. Рябко, М. П. Кондратенко.
15. Saleem Khawaja. Efficient suspended monorail locomotive transportation systems for underground mines // MiningTechnology, January 12, 2023. URL: https://www.mining-technology.com/sponsored/suspended-mining-locomotive-ferrit-dlz130f/
16. Klontz K. W., Divan D. M., Novotny D. W., Lorenz R. D. Contactless Power Delivery System for Mining Applications // IEEE Transactions on Industry Applications. – 1995. – Vol. 31. – No. 1. – pp. 27-35. DOI: 10.1109/28.363053.
17. Manual. Contactless Energy Transfer System. MOVITRANS® line Transfer System for TDM90E Flat Pickups. Project Planning. 31559441/EN, Jan. 2024. URL: https://download.sew-eurodrive.com/download/pdf/31559441.pdf#search=%22PLAA;PLA;PL;P%22

18. Costa V. S., Marques E., Mendes A. M., Perdigão M. S. Resonant converter topology impact on a Dynamic IPT application // 2021 Telecoms Conference (ConfTELE). IEEE. – 2021. – pp. 1-6.
19. Fujita T., Yasuda T., Akagi H. A Dynamic Wireless Power Transfer System Applicable to a Stationary System // IEEE Transactions on Industry Applications. – 2017. – Vol. 53. – No. 4. – pp. 3748-3757. DOI: 10.1109/TIA.2017.2680400.
20. Guo Y., Wang L., Zhu Q., Liao C., Li F. Switch-On Modeling and Analysis of Dynamic Wireless Charging System Used for Electric Vehicles // IEEE Transactions on Industrial Electronics. – 2016. – Vol. 63. – No. 10. – pp. 6568-6579. DOI: 10.1109/TIE.2016.2557302.
21. Zeng Rong, Onar Omer, Mohammad Mostak, Su Gui-Jia, Asa Erdem, Galigekere Veda Prakash. Modeling and Analysis of a Polyphase Wireless Power Transfer System for EV Charging Applications // IEEE Applied Power Electronics Conference and Exposition (APEC). IEEE, 2022. pp. 1871097. DOI: 10.1109/APEC43599.2022.9773533.
22. Foote A., Onar O. C. A review of high-power wireless power transfer // 2017 IEEE Transportation Electrification Conference and Expo (ITEC). IEEE, 2017. pp. 234-240.
23. Esteban B., Sid-Ahmed M., Kar N. C. A comparative study of power supply architectures in wireless EV charging systems // IEEE Transactions on Power Electronics. – 2015. – Vol. 30. – No. 11. – pp. 6408-6422.
24. Shevchenko V., Husev O., Strzelecki R., Pakhaliuk B., Poliakov N., Strzelecka N. Compensation topologies in IPT systems: Standards, requirements, classification, analysis, comparison and application // IEEE Access. – 2019. – Vol. 7. – pp. 120559-120580.
25. Zhang W., Mi C. C. Compensation topologies of high-power wireless power transfer systems // IEEE Transactions on Vehicular Technology. – 2015. – Vol. 65. – No. 6. – pp. 4768-4778.
26. Mude K. N., Aditya K. Comprehensive review and analysis of two-element resonant compensation topologies for wireless inductive power transfer systems // Chinese Journal of Electrical Engineering. – 2019. – Vol. 5. – No. 2. – pp. 14-31.
27. Xiaohui Qu, Hongdou Han, Siu-Chung Wong, Chi K. Tse, Wu Chen. Hybrid IPT topologies with constant current or constant voltage output for battery charging applications // IEEE Transactions on Power Electronics. – 2015. – Vol. 30. – No. 11. – pp. 6329-6337.
28. Shuyu Cao, Htet Ye Yint Naing, R.T. Naayagi, Sze Sing Lee, Feng Wei, King Jet Tseng. Wireless charging resonant converter topology study based on analytical design computation // 2020 3rd International Conference on Energy, Power and Environment: Towards Clean Energy Technologies. IEEE, 2021. pp. 1-6.
29. Aditya K., Williamson S. S. Design guidelines to avoid bifurcation in a series–series compensated inductive power transfer system // IEEE Transactions on Industrial Electronics. – 2018. – Vol. 66. – No. 5. – pp. 3973-3982.
30. Wang B., Hu A. P., Budgett D. Maintaining middle zero voltage switching operation of parallel–parallel tuned wireless power transfer system under bifurcation. IET Power Electronics. – 2014. – Vol. 7. – Iss. 1. – pp. 78-84.
31. Matteo Brunelli. Introduction to the Analytic Hierarchy Process. Springer Cham, 2015. 83 p. DOI: 10.1007/978-3-319-12502-2.
32. Algafri M., Alghazi A., Almoghathawi Y., Saleh H., Al-Shareef K. Smart City Charging Station Allocation for Electric Vehicles Using Analytic Hierarchy Process and Multiobjective Goal-programming // Applied Energy. – 2024. – Vol. 372. – pp. 123775. DOI: 10.1016/j.apenergy.2024.123775.

Конфликт интересов

Авторы заявляют об отсутствии конфликта интересов.

© 2026 Авторы. Издательство Кузбасского государственного технического университета имени Т.Ф. Горбачева. Эта статья доступна по лицензии CreativeCommons «Attribution» («Атрибуция») 4.0 Всемирная (https://creativecommons.org/licenses/by/4.0/)

Благодарность. Исследование выполнено при финансовой поддержке государственного задания Министерства науки и высшего образования Российской Федерации (№ 075-03-2024-082-2).

Информация об авторах

Завьялов Валерий Михайлович, докт. техн. наук, профессор, кафедра электроэнергетики
e-mail: VMZavyalov@sevsu.ru

Абейдулин Сергей Адельзанович, старший преподаватель, кафедра электроэнергетики e-mail: SAAbeidulin@sevsu.ru

Шайтор Николай Михайлович, канд. техн. наук, доцент, кафедра электроэнергетики
e-mail: shaytor1950@mail.ru

Севастопольский государственный университет
299053, Россия, г. Севастополь, ул. Университетская, 33

Семыкина Ирина Юрьевна, докт. техн. наук, старший научный сотрудник, лаборатория цифровой трансформации предприятий минерально-сырьевого комплекса
e-mail: semykinaiju@kuzstu.ru

Лебедев Геннадий Михайлович, доктор техн. наук, профессор, профессор кафедры электроснабжения горных и промышленных предприятий,
e-mail: lgm.egpp@kuzstu.ru

Кузбасский государственный технический университет имени Т.Ф. Горбачева
650000, Россия, г. Кемерово, ул. Весенняя, 28